arXiv:astro-ph/0010274v1 13 Oct 2000

Evidence for Rapid Iron K_α Line Flux Variability in MCG–6-30-15

Simon Vaughan

X-Ray Astronomy Group; University of Leicester; Leicester, LE1 7RH; United Kingdom

sav@star.le.ac.uk

and

Rick Edelson

Astronomy Department; University of California; Los Angeles, CA 90095-1562; USA

rae@astro.ucla.edu

ABSTRACT

This paper employs direct spectral fitting of individual orbital data in order to measure rapid X-ray iron K_α line and continuum spectral slope variations in Seyfert 1 galaxies with unprecedented temporal resolution. Application of this technique to a long *RXTE* observation of MCG−6-30-15 indicates that the line flux does vary on short ($\lesssim$1 d) timescales, but that these variations are *not* correlated with changes in the continuum flux or slope. These rapid variations indicate that the line does indeed originate close to the black hole, confirming predictions based on its very broad profile. However, the lack of a correlation with the continuum presents problems for models in which the line variations are driven by those in the continuum, modified only by light-travel time effects. Instead, it may be that the line responds according to a physical process with a different time scale, such as ionization instabilities in the disk, or perhaps that the geometry and physical picture is more complex than implied by the simplest disk–corona models.

These data also indicate that the slope of the underlying power-law continuum (Γ) shows strong variability and is tightly correlated with the continuum flux in the sense that the spectrum steepens as the source brightens. All of these results have been checked with extensive simulations, which also indicated that a spurious correlation between Γ and Compton reflection fraction (R) will result if these quantities are measured from the same spectra. This casts serious doubts on previous claims of such a $\Gamma - R$ correlation.

Subject headings: galaxies: active — galaxies: individual (MCG−6-30-15) — galaxies: Seyfert — X-rays: galaxies — methods: data analysis

1. Introduction

X-ray observations probe the innermost regions of Active Galactic Nuclei (AGN) and potentially offer a direct probe the immediate environment of the central, supermassive black holes thought to power AGN (e.g., Mushotzky, Done & Pounds 1993). The currently favored model for the central regions comprises a hot ($\sim 10^8 - 10^9$ K) optically-thin corona lying above and below the surface of an optically thick, geometrically thin accretion disk (e.g., Haardt & Maraschi 1993). Ultraviolet photons from the disk are inverse-Compton scattered to X-ray energies ('up-scattered') as they pass through the corona. The X-ray source, in turn, illuminates the accretion disk, with photons either absorbed and thermalized within the disk or 'reflected,' producing a characteristic reflection hump and strong iron K_α fluorescence (Lightman & White 1988; George & Fabian 1991).

Ginga observations showed these features to be common to Seyfert 1 nuclei and provided strong support for this model (Pounds et al. 1990; Nandra & Pounds 1994). However, the *ASCA* mission provided the first spectrally resolved iron K_α line profiles, showing that many Seyfert 1 galaxies to have a broad, redshifted iron line profiles (Tanaka et al. 1995; Nandra et al. 1997b), best explained by a combination of Doppler and gravitational redshifts from the inner regions of an accretion disk around a black hole (Fabian et al. 1995). These provide some of the best evidence in support of the black hole model (see reviews by Fabian et al. 2000 and Nandra 2000).

Such a compact region *should* respond very rapidly to changes in the illuminating flux (Stella 1990; Matt & Perola 1992). Simple models of X-ray illuminated accretion disks, in which the reprocessing time scale is very short, predict the line should respond to variations in the continuum with a delay of order the light-crossing time ($\sim 1000 M_7$ s at $20 r_g$ from a black hole of mass $10^7 M_7$ $M_\odot$, where $r_g = GM/c^2$). The response of the line to the continuum could then be used to deduce the geometry and absolute size scales of the inner accretion disk. This could in principle provide a more accurate method for estimating the mass of the central black hole and, when combined with accurate line profiles, even reveal its spin (Reynolds et al. 1999; Reynolds 2000).

In the case of MCG−6-30-15, the profile is so broad that most of the line flux appears to originate within $\sim 20 r_g$ of the black hole (Tanaka et al. 1995; Iwasawa et al. 1996; Guainazzi et al. 1999). Recent *Chandra* observations do not show any strong, narrow component to the iron line (Lee et al. 2000b), supporting the view that, in this object at least, most of the line flux originates close to the black hole. Attempts to measure the expected continuum flux driven variability of the iron line (Iwasawa et al. 1996, 1999; Lee et al. 2000a) have led to suggestions that the line may be variable, but also provide indications that the simple picture above may not fully explain the behavior.

The situation in other Seyfert 1s is even less clear. For instance, Nandra et al. (1999) found that in NGC 3516, another Seyfert 1 with a broad iron line, the core of the line profile (6.0–6.4 keV) appeared to track the continuum but the broad wings of the line varied in an uncorrelated fashion. In a long (30 d) observation, NGC 7469 showed marginal evidence for iron line variability correlated with X-ray flux (Nandra et al. 2000). Complex variability has also been reported in the iron lines

of NGC 4051 (Wang et al. 1999) and NGC 7314 (Yaqoob et al. 1996). Weaver, Gelbord & Yaqoob (2000) suggest that iron line variability is a common property in Seyfert 1s based on an analysis of archival *ASCA* data. On the other hand, Chiang et al. (2000) found no evidence for line variability in a simultaneous *RXTE*/*ASCA* observation of NGC 5548. However, recent *Chandra* observations of NGC 5548 revealed a strong, narrow component to the iron line, indicating that a significant fraction of the line flux originates in distant material (Yaqoob et al. 2000). A constant, narrow line is indeed predicted by AGN unification schemes (Krolik, Madau & Życki 1994; Ghisellini, Haardt & Matt 1994).

In order to determine if Seyfert 1 iron lines do indeed vary rapidly, we have designed a new analytical technique specifically to measure rapid changes in the X-ray spectrum by direct spectral fitting to the individual orbital data. This has then been applied to MCG−6-30-15, an ideal subject for this approach because it is a bright, highly variable Seyfert 1 with an unambiguously broad iron line and a very long (8 d), quasi-continuous *RXTE* observation.

The rest of the paper is organized as follows. In the next section the observations and data reduction procedures are described. The spectral analysis is discussed in § 3 and the results of this analysis are tested using extensive simulations in § 4. The implications of the results of are discussed in § 5, followed by a brief summary of the main results in § 6.

2. Observations and Data Reduction

MCG−6-30-15 was observed by *RXTE* during the period 1997 August 4 – 12. Further details of the observation and an analysis of the time-averaged spectral properties are given by Lee et al. (1999). The *RXTE* observations were taken simultaneously with *ASCA* (Iwasawa et al. 1999; Lee et al. 2000a), but because the *ASCA* count rate is a factor ~ 10 less than that of *RXTE* these data are not as useful for measuring rapid spectral variability. The *ASCA* data were therefore not used in the present analysis.

The *RXTE* Proportional Counter Array (PCA) consists of five collimated Proportional Counter Units (PCUs), sensitive to X-rays in a nominal 2–60 keV bandpass and with a total collecting area of ~ 6250 cm^2. PCU units 3 and 4 were turned off during most of the observation due to performance problems and here only data from three of the PCUs (0, 1 and 2) were used. In the following analysis, data from the top (most sensitive) layer of the PCU array were extracted using the `REX` reduction script and `SAEXTRCT v4.2b`. Poor quality data were excluded on the basis of the following acceptance criteria: the satellite has been out of the South Atlantic Anomaly (SAA) for at least 30 min; Earth elevation angle $\geq 10^\circ$; offset from optical position of MCG−6-30-15$\leq 0.02^\circ$; and `ELECTRON0`≤ 0.1. This last criterion removes data with high anti-coincidence rate in the propane layer of the PCUs. These selection criteria left a total of 326 ks of good data. The background was estimated using the latest version of the 'L7–240' model (Jahoda et al. 2000), specifically the model files `pca_bkgd_faint240_e3v19990909.mdl` and `pca_bkgd_faintl7_e3v19990824.mdl` have

been used[1].

Light curves were initially extracted from the `STANDARD-2` data with 16 s time resolution. The data were rebinned on orbital sampling period (5760 s) of *RXTE*, with the Earth-occultation gaps as the bin edges. This has the advantage of improving the signal-to-noise and sampling the data on the shortest available uninterrupted timescale. A total of 123 orbits of data were extracted. Three of these contain less than 1 ks of good data and less than 10^4 source counts, and were excluded on this basis. The remaining 120 'good' orbits each contain $1.4 - 3.7$ ks of good exposure time and $1.2 - 6.1 \times 10^4$ source counts. Source and background spectra were extracted from each of these 120 orbits. Response matrices were generated throughout the length of the observation using `PCARSP v2.43`, but over such a short duration the response does not change significantly. In the following spectral analysis a response matrix taken from the middle of the observation was used.

3. Spectral Analysis

The goal of this analysis is to measure the variability properties of the iron line and continuum with the highest possible temporal resolution. As discussed above, the natural sampling rate is the satellite orbital period (96 min), as that is the shortest timescale on which no regular interruptions in the light curve occur. Once the data were individually extracted and calibrated for each of the 120 good orbits, they were then fitted using the `XSPEC` v11.01 (Arnaud 1996) software package. The key to keeping this process robust was to utilize the minimum number of free parameters needed to produce an acceptable fit (e.g., $\chi^2_\nu \approx 1$) in each orbit. The process of determining what spectral model to use is discussed in the next two subsections, and the errors are estimated and final data are presented in the following two subsections. Simulated data were then used to test this approach under a variety of conditions, as discussed in the following section.

3.1. Time-Averaged Spectral Fits

MCG−6-30-15 is known to contain strong warm absorber features (Nandra & Pounds 1992; Reynolds et al. 1995; George et al. 1998). In order to reduce the effect of this on the spectral analysis data below 3 keV were ignored (see Figure 1 of Iwasawa et al. 1996). This has the additional benefit of avoiding possible calibration problems with the PCA below 3 keV. The data were further restricted to energies less than 18 keV, above which the source count rate is too low to obtain a good detection in each orbit.

The spectral models were produced by fitting the time-averaged *RXTE* spectrum (Figure 1). In each trial model the neutral absorption column was fixed at the Galactic value, i.e., $N_H =$

[1]See `http://lheawww.gsfc.nasa.gov/~keith/dasmith/rossi2000/index.html`

4.09×10^{20} cm^{-2}, which Lee et al. (1999) found to be consistent with the *RXTE* spectrum. (Such a small column has a negligible effect on the spectrum above 3 keV.) The time-averaged spectrum shows clear residuals when compared to a simple power-law (Figure 1b). The strongest residual feature peaks at ~ 6 keV and is due to the iron K$_\alpha$ line. In addition to this the spectrum shows a significant up-turn above 10 keV characteristic of a Compton reflection hump (Figure 1b,c). Therefore the first trial spectral model (Figure 1d) comprised a power-law, a broad Gaussian emission line and a `pexriv` reflection component (Magdziarz & Zdziarski 1995). The inclination angle of the reflector was fixed at 30°, and the e-folding energy of the incident power-law was fixed at 100 keV, consistent with the previous fits of Tanaka et al. (1995), Guainazzi et al. (1999) and Lee et al. (1999).

This model provides a statistically unacceptable fit to the time-averaged spectrum but, as can be seen in Figure 1d, the data/model residuals are at the $\lesssim 3$ % level, which is about the limit of the PCA calibration[2]. Also, the energy resolution of the PCA (~ 1 keV at 6 keV) makes the PCA largely insensitive to the detailed profile of the iron line, and therefore a Gaussian is a good approximation. For these reasons this model was accepted as a reasonable parameterization of the time-averaged spectrum. The fit parameters were: power-law slope $\Gamma = 2.06$; line energy $E_{K\alpha} = 5.73$ keV, normalization $F_{K\alpha} = 2.17 \times 10^{-4}$ photons cm^{-2} s^{-1}, width $\sigma_{K\alpha} = 0.87$ keV and equivalent width $EW_{K\alpha} = 374$ eV; relative reflection strength $R = 1.42$.

3.2. Time-Resolved Spectral Fits

The above model has been fitted to all 120 orbital spectra. Even in these short observations, with only ~ 2.5 ks integration times, the line was always well detected. As with the time-averaged spectrum, the addition of a Gaussian line significantly improved the fits to the individual orbital spectra ($\gtrsim 99.9\%$ level in an F-test) compared to a simple power-law model. However, the reflection component was not nearly as well detected in each orbit (only $\sim 99\%$ confidence).

The F-test was used to decide what free parameters to include in the fit. The spectral fits were repeated with the parameters $(\Gamma, F_{K\alpha}, R)$ kept fixed at their time-averaged values (as given above). The difference in total χ^2 between the fits when a given parameter was fixed and when all parameters were free was then used to assess the significance of allowing that parameters to be free. The F-statistic values are 1.59, 1.51 and 1.08, respectively, for 120 additional parameters. These results indicate that the inclusion of Γ and $F_{K\alpha}$ as free parameters in the orbital fits is justified, but that there is no justification for including R as a free parameter. On the basis of this test and the simulations of § 4, allowing R to vary was not justified, so it was kept fixed at its time-averaged value in the following spectral fits. This situation might be physically realized if the reflecting material is very close to the X-ray source. The inclusion of line energy as a free parameter was

[2]See `http://lheawww.gsfc.nasa.gov/users/~keith/rossi2000/energy_response.ps`

also not justified. None of the spectral models used in this analysis included a constant, narrow component to the iron line as neither the *ASCA* observations nor the *Chandra* observations suggest the presence of such a feature (Lee et al. 2000b).

Lee et al. (1999) suggest that the elemental abundances of the reprocessor in MCG−6-30-15 differ from solar. To check that the spectral variability results presented here are not an artifact of using incorrect element abundances, the spectral fitting was repeated using the abundances of Lee et al. (1999). Specifically, iron was assumed to be over-abundant by a factor 2 while lighter elements were under-abundant by the same factor. Using this model the absolute values of the fit parameters changed slightly but the pattern of variability described below was essentially unchanged.

3.3. Error Estimation

Fitting this simple model to all 120 orbital spectra gave unusually low values of the fit-statistic, with $\chi^2_\nu < 1.0$ in 114 of the fits. This is most likely a result of the error bars on the net (source minus background) spectrum being overestimated. As discussed by Nandra et al. (2000), the standard software calculates errors on the net spectrum by combining errors on the total spectrum with those on the model background spectrum. The errors on the background are calculated using Poisson statistics on the background model, which will tend to overestimate the true uncertainty on the background in the case of short exposures, since the model is derived from a large amount of blank-sky data. For the purpose of assessing the variability of the measured parameters of MCG−6-30-15, all errors produced by the standard software have been ignored and new (1σ) errors were calculated based on the properties of the derived light curves. The errors on the source count rate were derived from the error on the mean of the ~ 150 individual 16s points within each orbital bin.

For the spectral fit parameters, where 16s data were not available, the errors have been calculated based on the properties of the orbital light curves. Specifically, the error, σ, on a given parameter was calculated from the point-to-point variance of the light curve for that parameter using the following equation:

$$\sigma^2 = \frac{1}{2}\frac{1}{N-1}\sum_{i=1}^{N-1}(x_i - x_{i+1})^2$$

where x_i are the N points in the light curve.

Simulations of constant light curves with known errors confirmed that the above equation gives an accurate representation of the errors in this situation (see also § 4). These are in fact conservative error estimates: in the absence of intrinsic variability, the point-to-point scatter in a light curve will be due only to measurement errors. If the source has intrinsic variations on such short time scales, the true error will be smaller than this because part of the scatter is due to those intrinsic variations. However, even these conservative error estimates cannot account for systematic

errors. Among these are the unlikely but conceivable possibilities that rapid changes in the spectral response of the PCA, or in the energy and depth of an iron K edge (from e.g., the warm absorber) could mimic the observed line variations.

The error on the power-law slope derived from the point-to-point scatter was $\sigma_\Gamma = 0.059$, which compares to a mean error of 0.028 from the standard software. For the iron line flux the error derived was $\sigma_{Fe} = 3.4 \times 10^{-5}$ photon cm^{-2} s^{-1}, compared to 4.3×10^{-5} from the standard software.

3.4. Spectral Variability Results

The light curves derived by fitting all 120 orbital spectra are shown in Figure 2, with error bars calculated as in the previous section. The top panel shows strong, rapid variations in the 2–10 keV count rate, F_{2-10}, which was assumed to be representative of the continuum flux of the source (see Nowak & Chiang 2000 and Lee et al. 2000a for detailed analyses of this light curve). The power-law slope appears significantly variable; a χ^2–test against a constant hypothesis gave χ^2=261.2 / 119 *dof*, corresponding to a rejection of the constant hypothesis at 99.99 % confidence. The iron line flux also shows significant variability, with χ^2=196.1 / 119 *dof* (significant at 99.9 %). Again, it is noted that these χ^2 values were calculated using the conservative errors discussed earlier.

Figure 3 shows the zero-lag correlation diagrams for these light curves. Two non-parametric statistics were employed to test for correlations, namely the Spearman rank-order correlation coefficient r_s and the Kendall τ_K–statistic (see e.g., Press et al. 1992). Only one correlation was significant, that between F_{2-10} and Γ, with $r_s = 0.778$ and $\tau_K = 0.587$, which differ from zero with significance levels $< 10^{-20}$. The correlation coefficients for F_{2-10} against $F_{K\alpha}$ were $r_s = 0.076$ and $\tau_K = 0.043$ and for Γ against $F_{K\alpha}$ they were $r_s = 0.056$ and $\tau_K = 0.037$, consistent with no correlation below the 40% level.

This tendency for the X-ray spectrum to steepen as the source gets brighter has been observed in many Seyfert 1s (e.g., Nandra et al. 1991; Ptak et al. 1994; Nandra et al. 1997a; Markowitz & Edelson 2000). However, it has not been clear whether this is due to intrinsic changes in the slope of the underlying power-law or the superposition of a constant reflection component on a power-law of constant slope but varying normalization. The inclusion of (fixed R) reflection in the above spectral fitting suggests that the Γ-flux correlation is genuine in MCG−6-30-15. As a check the above fits were repeated using a reflection component of fixed absolute flux (i.e., slope and normalization of the power-law incident on the reflector held constant), as might be expected if the reflecting material is very distant and responds only to the time-averaged continuum. The fits again show a strong Γ-flux correlation.

The correlation diagrams of Figure 3 show that the iron line flux is not correlated with the source flux nor with Γ. The rapid variations in the line flux do however suggests that the majority of the line flux does indeed originate in a compact region. Indeed, while the iron line is not as

strongly variable as the continuum, it does appear variable on time scales $\sim 0.5 - 2$ d, which is the shortest time for a factor of two change (e.g. day 665). In order to search for possible time-delays between the continuum and line, temporal cross-correlation functions were computed using both the interpolated correlation function (ICF; White & Peterson 1994) and the discrete correlation function (DCF; Edelson & Krolik 1988).

Figure 4 shows the cross-correlation functions. In these plots a positive time shift corresponds to the first quantity (i.e. F_{2-10}) leading the second. Both the ICF and DCF for F_{2-10} against Γ reach maximum correlation coefficients of $r_{max} = 0.80$ at zero-lag. The correlation functions for F_{2-10} against $F_{K\alpha}$ reach peaks at $\tau = +1.4$ day (continuum flux leading line), although in both cases the maximum correlation coefficient is small ($r_{max} = 0.50$ and 0.42 for the ICF and DCF, respectively).

The apparent lack of a strong correlation between the continuum and line fluxes is difficult to explain in the context of the standard model, as discussed in § 5.

4. Simulated Spectra

In order to assess the robustness of this spectral analysis, simulated data were produced to resemble as closely as possible the real data, and then analyzed in an identical fashion. Each simulated dataset consisted of 120 spectra produced using spectral models together with response matrices, exposure times and background spectra taken from the real data. Poisson noise was added to the total (source plus background) spectra and the entire simulated dataset was then fitted in exactly the same fashion as the real data. As the intention here was to produce simulated data which matched the properties of the real data as closely as possible, the original background files, which were derived from a model, not observed photons, were used in the fitting without Poisson noise added. This meant that net spectra produced from the simulated data also had systematically overestimated error bars (see § 3.3). For each test 10 complete sets of 120 spectra were produced.

4.1. Iron Line Simulations

The spectral models used to produce the simulated data were created with parameters derived from fits to the real data. For example, the first set of simulated data contains a variable continuum but constant iron line. The spectral models used to produce these simulated data were obtained by fitting the real data, then setting $F_{K\alpha}$ to its time-averaged value before the simulated spectra were generated. Thus, the simulated data should have had spectra with continuum slopes and normalizations that varied like the real data, but line fluxes that remained constant.

These constant-line simulations were used to justify the error estimation of § 3.3. With the errors calculated from the point-to-point scatter, each simulation gave $\chi^2_\nu \approx 1.0$ against a constant

hypothesis (from 10 simulations the mean χ^2_ν was 1.01 with a standard deviation of 0.09), indicating that this method does indeed provide a good estimate of the measurement error. The difference in χ^2 between the real data and the constant-line simulations suggested that the measured variability in the line is highly significant ($\chi^2_\nu = 1.64$ for the real data). Figure 5 shows the correlation diagrams from one of the constant-line simulations.

With the errors calculated using the standard software there is still a significant difference in χ^2 between the real data and the constant line simulations. Performing the χ^2–test as above but using the standard errors gave a $\chi^2_\nu = 1.05$ for the real data and $\chi^2_\nu \approx 0.65$ for the constant-line simulations. As the light curve for a constant line should have $\chi^2_\nu = 1$ if the errors are correct, the fact that the simulations gave $\chi^2_\nu \approx 0.65$ again reinforces the view that the standard errors are overestimates, and the recalculated errors are more accurate.

Simulations have also been generated in which the line flux follows the continuum flux with zero lag (i.e., $F_{K\alpha}$ is a linear function of power-law normalization). In these simulations the equivalent width of the line is approximately constant. Again, fits to these simulated data recovered the input values accurately and this time showed the expected strong correlation between line flux and continuum flux (see Figure 6).

These simulations suggest that the two simplest hypotheses for the behavior of the iron line, namely a constant flux or a constant equivalent width, can be rejected in the case of MCG−6-30-15.

4.2. Continuum Simulations

These simulations also reveal a bias in the simultaneous determination of Γ and R from these data. Figure 7 shows the results of fitting a simulated dataset in which the model (input) R was held constant. In order to test how accurately Γ and R can be simultaneously constrained, R was left as a free parameter When fitting the simulated data in this test. There is a clear tendency for the value of R measured from the fit to increase with Γ. The correlation coefficients are $r_s = 0.739$ and $\tau_K = 0.554$, both indicating that Γ and R are correlated with very high significance. As R is known to be constant in these simulated data, this can only be an artifact of the fitting procedure. Chiang et al. (2000) and Nandra et al. (2000) have previously discussed this effect in the context of their respective spectral variability analyses. On the basis of these simulations it is concluded here that this effect is an artifact of the interdependency of the two model components, power-law and reflection, and that it is not possible to simultaneously measure both Γ and R from the real data in an unbiased fashion. The implications of this bias for previous studies is discussed in § 5.

A secondary point is that such a correlation introduced by the fitting procedure is not the source of the observed correlation between Γ and F_{2-10}, which persists independent of the inclusion of fixed (absolute or relative) reflection in the fit.

5. Discussion

This paper presents time-resolved X-ray spectroscopy of MCG−6-30-15 with a resolution of 96 min. On these timescales there is evidence that the iron line flux is variable but does not appear to be simply related to the observed continuum flux. Also, the slope of the underlying power-law continuum varies significantly and appears to be correlated with the source flux in the sense that the power-law steepens as the source luminosity increases. Extensive simulations have been used to assess the robustness of these results and search for possible sources of error in the line determination; none were found. That said, it is not possible to rule out the influence of subtle systematic effects with arbitrary confidence, as discussed earlier. While these seem unlikely, confirmation of the observed iron line variability must come from missions such as *XMM-Newton* which offer high throughput and spectral resolution far in excess of *RXTE*. However, for the purpose of the following discussion, the measured line variations are assumed to be intrinsic to the source.

5.1. Reconciliation with Previous Analyses

The temporal properties of the iron line in MCG−6-30-15 have previously been addressed by Iwasawa et al. (1996, 1999), Lee et al. (2000a) and Reynolds (2000). With the line properties measured as a function of time throughout an observation (e.g. § 3.2 of Iwasawa et al. 1996) the line flux appeared variable on timescales $\sim 4 \times 10^4$. However, when the observations were broken into intervals of high and low fluxes they did not show the expected correlation between the line flux and continuum, and even variability of the line was difficult to detect (Lee et al. 2000a). Reynolds (2000) used an interpolation procedure to search for lags or leads between a continuum band (2–4 keV) and the line band (5–7 keV) but found none.

The fully time-resolved spectral analysis presented in this paper suggests that the line flux is indeed variable on short timescales ($\sim$ 1 d) but is not correlated with the continuum over the duration of the observation, thus accounting for the apparent lack of line variability seen in the flux-correlated analyses. A further point is that the lack of correlation between line and continuum, combined with smaller amplitude variations in the line than the continuum, is responsible for the anti-correlation between line equivalent width and continuum luminosity observed by Lee et al. (2000a).

5.2. Rapid Iron Line Variability

This lack of a correlation between the line flux and continuum suggests that the reprocessing is more complex than that needed to produce a strong reverberation signature (Blandford & McKee 1982). Some obvious possibilities that could affect the response of the line include the non-negligible size of the X-ray emitting region(s) compared to the inner disk, the presence of a strongly ionized

layer on the surface of the disk (Ross, Fabian & Young 1999; Nayakshin 2000), the orbital motion of both the X-ray emitting region and the disk material (Ruszkowski 1999), and the geometry of the inner disk (e.g. Blackman 1999).

Perhaps the most promising of these is the effect of an ionized skin on the properties of the iron K_α line. It is likely that the bulk of the line flux in MCG−6-30-15 originates in the deeper, relatively neutral layers of the disk since the line appear neutral. Scattering in an overlying, ionized skin can be effective at degrading the strength of the neutral iron line, as discussed by Nayakshin & Kallman (2000) and Nayakshin (2000). The temperature and optical depth of the ionized skin, which are functions of the geometry and spectrum of the X-ray source, thus have a strong effect on the observed strength of the line. It is interesting to note this means it is in principle possible for the line flux to change without there being any change in the continuum over the *RXTE* bandpass. This is because the temperature of the ionized skin is a function of the energy at which the X-ray spectrum rolls over (see § 6.3.2 of Nayakshin & Kallman 2000) and the strength of ultraviolet bump, neither of which are observed by *RXTE* but could be (and most likely are) variable. Alternatively the physical conditions of the accretion disk skin could be governed by some process other than photoionization. One strong candidate is mechanical heating from the magnetohydrodynamic turbulence intrinsic to the disk, which may also be responsible for the formation of the disk corona (e.g. Miller & Stone 2000).

Based on the X-ray variability of MCG−6-30-15, Iwasawa et al. (1996) and Fabian (1997) suggested that the X-ray source at any given time consists of a few discrete flaring regions each illuminating a relatively small area of the disk. This 'patchy' geometry makes modelling the response of the line to the continuum difficult, especially if the flaring regions are close to the disk surface (Nayakshin 2000). Directly following an X-ray flaring event the accretion disk surface, at least in the immediate vicinity of the flare, is likely to be out of hydrostatic equilibrium, and the timescale for the material to return to equilibrium is long compared to the light-crossing time (Nayakshin et al. in prep.). During periods when the disk surface is out of equilibrium the line emission would be poorly correlated with the driving continuum due to ionization instabilities. The line emission may therefore only correlate with the continuum emission on timescales much longer than the expected light-crossing time, which will average out the effects of orbital modulation and instabilities. For example, if the source were to enter a prolonged low state (as recently seen in NGC 4051; Uttley et al. 1999) then the iron line flux should eventually respond. Thus it is important to measure spectral variability on long as well as short time scales in order to understand the response of the iron K_α line to the continuum. An alternative, if rather speculative explanation for the unusual line variations,, is that one of the basic assumptions about the production of the broad iron line by reflection off a geometrically thin, optically thick accretion disk is flawed.

5.3. Continuum Slope Variability

The strong correlation between X-ray flux and underlying spectral slope found in MCG−6-30-15 can be disentangled from the effects of reflection. Similar effects have been observed in NGC 5548 (Chiang et al. 2000), NGC 7469 (Nandra et al. 2000) and IC 4329a (Done, Madejski & Życki 2000), although in the case of NGC 7469, at least on timescales of days, the power-law slope appeared better correlated with the ultraviolet luminosity than the X-ray luminosity.

These results imply that some property of the X-ray emitting corona (e.g. electron temperature, optical depth, size) is changing with the X-ray flux, although at this stage it is not clear which one it is. Various authors have investigated the spectral variability properties of accretion disk coronae for both AGN and Galactic accreting sources (e.g. Haardt, Maraschi & Ghisellini 1997; Poutanen & Fabian 1999; Malzac & Jourdain 2000). In these models the simplest way to produce a slope-flux correlation similar to that observed in MCG−6-30-15 is if the X-ray variability is driven by changes in the seed photon population (e.g. § 5 of Malzac & Jourdain 2000). This possibility is consistent with the tentative claim that the EUV flux in NGC 5548 leads the hard X-ray flux by $\sim 10 - 30$ ks (Chiang et al. 2000).

5.4. Compton Reflection and Other Spectral Components

Another use of spectral variability to study AGN physics is to search for a relation between the strength of the Compton reflection component and other properties. The strength of the Compton reflection component could in principle provide an independent diagnostic of the geometry/albedo of the disk. A recent example is the result of Zdziarski, Lubiński & Smith (1999), who find a correlation between Γ and R measured in a sample of Seyfert galaxies. If confirmed, such a correlation would suggest that there is significant feedback between the X-ray source and the reprocessing medium.

Unfortunately, the *Ginga* and *RXTE* data gathered to date cannot provide good constraints on R on short timescales. In fact, the simulations of § 4.2 show that there is a serious bias in the simultaneous determination of Γ and R that leads to a strong, false correlation between these two parameters. A similar effect was discussed by Chiang et al. (2000), Nandra et al. (2000) and Matt (2000). The spurious correlation found in the simulations in the current paper (see § 4.2) spans almost the entire range of parameter space probed by Zdziarski et al. (1999) in their study of a sample of Seyfert galaxies, and indicates that the question of whether Γ and R are intrinsically correlated, as suggested to be the case by those authors, remains open. A corollary of this is that other correlations involving R may be biased by this effect. For example, the anti-correlation between line equivalent width and R noted by Chiang et al. (2000) and Lee et al. (2000a) may be due to a combination of an intrinsic Γ-flux correlation, a relatively constant iron line flux and a spurious correlation between Γ and R. In this case the line equivalent width would appear to anti-correlate with Γ and hence with R. These results highlight the difficulties in simultaneously fitting two broad continuum components from data of limited band-pass. A final point is that

the line measurements shown in Figure 2 remain largely unchanged if R is left free in the spectral fitting. The main results of this paper are therefore not strongly affected by the presence of a genuine correlation between R and Γ (which would be accounted for in the free-R fits).

6. Conclusions

This paper presents a new method of analyzing Seyfert 1 X-ray variability data, designed to measure rapid spectral variations by fitting data from individual orbits. This was applied to a long (8 d) *RXTE* observation of the bright, strongly variable Seyfert 1 galaxy MCG−6-30-15, and the conclusions were tested with extensive simulations. This provided the clearest evidence to date that the iron line flux ($F_{K\alpha}$) of a Seyfert 1 varies on relatively short ($\lesssim$1 d) timescales. However, the variations were *not* correlated with or simply related to the continuum variations. As the line is very broad, indicating that the bulk of the flux is produced close to the black hole, the lack of correlation contradicts the simplest picture in which the line variations are driven by variations in a point-like continuum source, modulated by light-travel effects. Although many modifications to this standard picture are possible, one reasonable solution is that the line variations are dominated by some other process, for instance, ionization instabilities, in which case the dominant timescale would be that for the system to return to equilibrium. Another is that there is something wrong with the simple disk-corona picture described above. In any event this result indicates that the physics of reprocessing in the central engine is more complex than previously thought.

The slope of the underlying X-ray power-law (Γ) shows strong variability and is tightly correlated with the source flux in the sense that the power-law steepens as the source gets brighter.

This behaviour indicates that the properties of the corona are rapidly variable and, if Compton-cooling is the dominant process in determining the X-ray spectral slope, may be driven by variations in the unobserved EUV band. The limited band-pass of these data and intrinsic bias in the simultaneous measurement of Γ and R appear to conspire to produce a spurious correlation between these two quantities. This strongly supports the conclusions of previous works (e.g., Nandra et al. 2000) that indicates that the correlation claimed in Zdziarski et al. (1999) may be an artifact of the analysis.

The unexpected result concerning the iron line variability hint at much more complex behavior than expected in Seyfert 1s. *XMM-Newton*, with its unprecedented combination of high throughput and spectral resolution, is ideally suited to study rapid iron line variability. We eagerly await the results of the long observations of this and other Seyfert 1s that will soon be made by *XMM-Newton*.

It is a pleasure to thank Tess Jaffe and the members of the *RXTE* GOF for assistance with the data reduction, Alex Markowitz for help with the cross-correlation functions and Keith Arnaud for help with `XSPEC`. We are also grateful to Sergei Nayakshin, Bob Warwick and Chris Reynolds for valuable discussions. This research made use of data obtained from the High Energy Astrophysics

Science Archive Research Center (HEASARC), provided by NASA's Goddard Space Flight Center. SV acknowledges support from PPARC and RE acknowledges support from NASA grants NAG 5-7317 and NAG 5-9023.

REFERENCES

Arnaud, K. 1996, in: *Astronomical Data Analysis Software and Systems*, Jacoby, G., Barnes, J., eds., ASP Conf. Series Vol. 101, p17

Blandford, R. D., McKee, C. F. 1982, ApJ, 255, 419

Blackman, E. G. 1999, MNRAS, 306, L25

Chiang, J., Reynolds, C. S., Blaes, O. M., Nowak, M. A., Murray, N., Madajski, G., Marshall, H. L., Magdziarz, P. 2000, ApJ, 528, 292

Done, C., Madejski, G. M., Życki, P. T. 2000, ApJ, 536, 213

Edelson, R., Krolik, J. H. 1988, ApJ, 333, 646

Fabian, A. C. 1997, in *X-Ray Imaging and Spectroscopy of Cosmic Hot Plasmas*, ed. F. Makino & K. Mitsuda (Tokyo: Universal Academy Press), 201

Fabian, A. C., Nandra, K., Reynolds, C. S., Brandt, W. N., Otani, C., Tanaka, Y., Inoue, H., Iwasawa, K. 1995, MNRAS, 277, L11

Fabian, A. C., Iwasawa, K., Reynolds, C. S., Young, A. J. 2000, PASP, 112, 1145

George, I. M., Fabian. A. 1991, MNRAS, 249, 352

George, I. M., Turner, T. J., Netzer, H., Nandra, K., Mushotzky, R. F., Yaqoob, T. 1998, ApJS, 114, 73

Ghisellini, G., Haardt, F., Matt, G. 1994, MNRAS, 267, 743

Guainazzi, M., et al. 1999, A&A, 341, L27

Haardt, F., Maraschi, L. 1993, ApJ, 413, 507

Haardt, F., Maraschi, L., Ghisellini, G. 1997, ApJ, 476, 620

Iwasawa, K., et al. 1996, MNRAS, 283, 1038

Iwasawa, K., Fabian, A. C., Young, A. J., Inoue, H., Matsumoto, C. 1999, MNRAS, 306, L19

Jahoda, K., et al. 2000, in preparation

Krolik, J. H., Madau, P., Życki, P. T. 1994, ApJ, 420, L57

Lee, J. C., Fabian, A. C., Brandt, W. N., Reynolds, C. S., Iwasawa, K. 1999, MNRAS, 310, 973

Lee, J. C., Fabian, A. C., Reynolds, C. S., Brandt, W. N., Iwasawa, K. MNRAS, 2000a, in press (astro-ph/9909239)

Lee, J. C., et al. , 2000b, in prep.

Lightman, A. P., White, T. R. 1988, ApJ, 335, 57

Magdziarz, P., Zdziarski, A. A. 1995, MNRAS, 273, 837

Malzac, J., Jourdain, E. 2000, A&A, 359, 843

Markowitz, A., Edelson, R. 2000, ApJ, in press (astro-ph/0009422)

Matt, G., Perola, G. C. 1992, MNRAS, 259, 433

Matt, G. 2000, to appear in the proceedings of *X- Ray Astronomy '99* (astro-ph/0007105)

Miller, K. A., Stone, J. M. 2000, ApJ, 534, 398

Mushotzky, R.F., Done, C., Pounds, K.A. 1993, ARA&A, 31, 717

Nandra, K., Pounds, K. A., Stewart, G. C., George, I. M., Hayashida, K., Makino, F., Ohashi, T. 1991, MNRAS, 248, 760

Nandra, K., Pounds, K. A. 1992, Nature, 359, 215

Nandra, K., Pounds, K. A. 1994, MNRAS, 268, 405

Nandra, K., George, I., Mushotzky, R., Turner, T. J., Yaqoob, T. 1997a, ApJ, 476, 70

Nandra, K., George, I., Mushotzky, R., Turner, T. J., Yaqoob, T. 1997b, ApJ, 477, 602

Nandra, K., George, I. M., Mushotzky, R. F., Turner, T. J., Yaqoob, T. 1999, ApJ, 523, L17

Nandra, K., Le, T., George, I. M., Edelson, R. A., Mushotzky, R. F., Peterson, B. M., Turner, T. J. 2000, ApJ, in press (astro-ph/0006339)

Nandra, K. 2000, to appear in the proceedings of *X-Ray Astronomy '99* (astro-ph/0007356)

Nayakshin, S. 2000, ApJ, in press (astro-ph/0005603)

Nayakshin, S., Kallman, T. 2000, ApJ, in press (astro-ph/0005597)

Nowak, M. A., Chiang, J. 2000, ApJ, 531, L13

Pounds, K. A., Nandra, K., Stewart, G. C., George, I. M., Fabian, A. C. 1990, Nature, 344,132

Poutanen, J., Fabian, A. C. 1999, MNRAS, 306, L31

Press, W. H., Teukolsky, S. A., Vetterling, W. T., Flannery, B. P. 1992, *Numberical Recipes*, Cambridge Univ. Press

Ptak, A., Yaqoob, T., Serlemitsos, P. J., Mushotzky, R., Otani, C. 1994, ApJ, 436, L31

Reynolds, C. S. 1999, ApJ, 533, 811

Reynolds, C. S., Fabian, A. C., Nandra, K., Inoue, H., Kunieda, H., Iwasawa, K. 1995, MNRAS, 277, 901

Reynolds, C. S., Young, A. J., Begelman, M. C., Fabian, A. C. 1999, ApJ, 514, 164

Reynolds, C. S., 2000, to appear in *Probing the Physics of Active Galactic Nuclei* (astro-ph/0009503)

Ross, R. R., Fabian, A. C., Young, A. J. 1999, MNRAS, 306, 461

Ruszkowski, M. 1999, MNRAS, 315, 1

Stella, L. 1990, Nature, 344, 747

Tanaka, Y., et al. 1995, Nature, 375, 659

Uttley, P., McHardy, I. M., Papadakis, I. E., Guainazzi, M., Fruscione, A. 1999, MNRAS, 307, L6

Wang, J. X., Zhou, Y. Y., Xu, H. G., Wang, T. G. 1999, ApJ, 516, L67

Weaver, K. A., Gelbord, J., Yaqoob, T. 2000, ApJ, in press (astro-ph/0008522)

White, R. J., Peterson, B. A. 1994, PASP, 106, 879

Yaqoob, T., Serlemitsos, P. J., Turner, T. J., George, I. M., Nandra, K. 1996, ApJ, 470, L27

Yaqoob, T., George, I. M., Nandra, K., Turner, T. J., Serlemitsos, P. J., Mushotzky, R. F. 2000, ApJ, in press (astro-ph/0008471)

Zdziarski, A. A., Lubiński, P., Smith, D. A. 1999, MNRAS, 303, L11

This preprint was prepared with the AAS LaTeX macros v5.0.

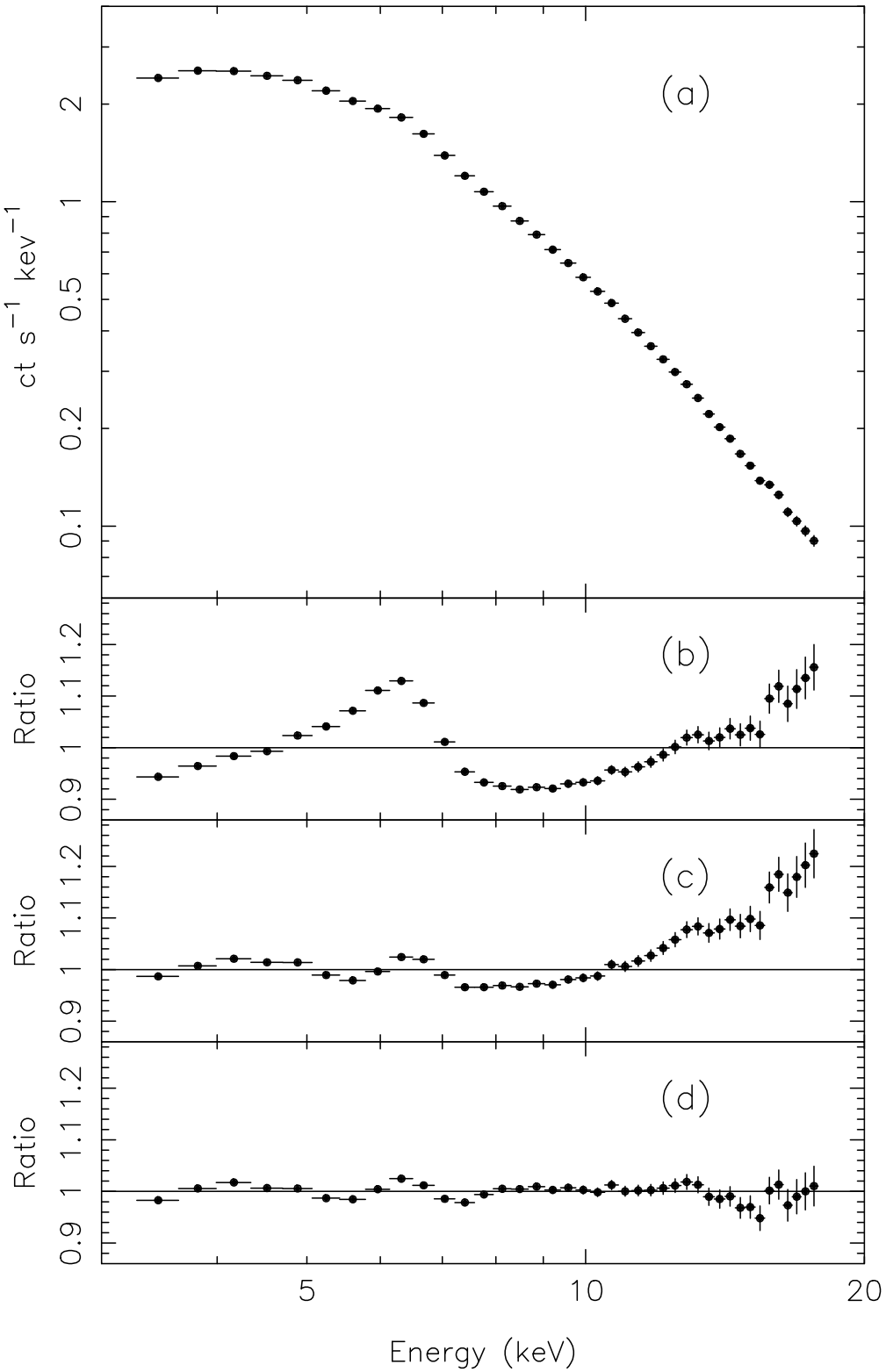

Fig. 1.— Time-averaged *RXTE* PCA spectrum of MCG−6-30-15. Panel *a* shows the count spectrum. Panels *b*, *c* and *d* show the data/model ratios when compared to various models. Panel *b* uses a simple power-law model, panel *c* uses a power-law plus broad Gaussian line and panel *d* uses a power-law, line and reflection component.

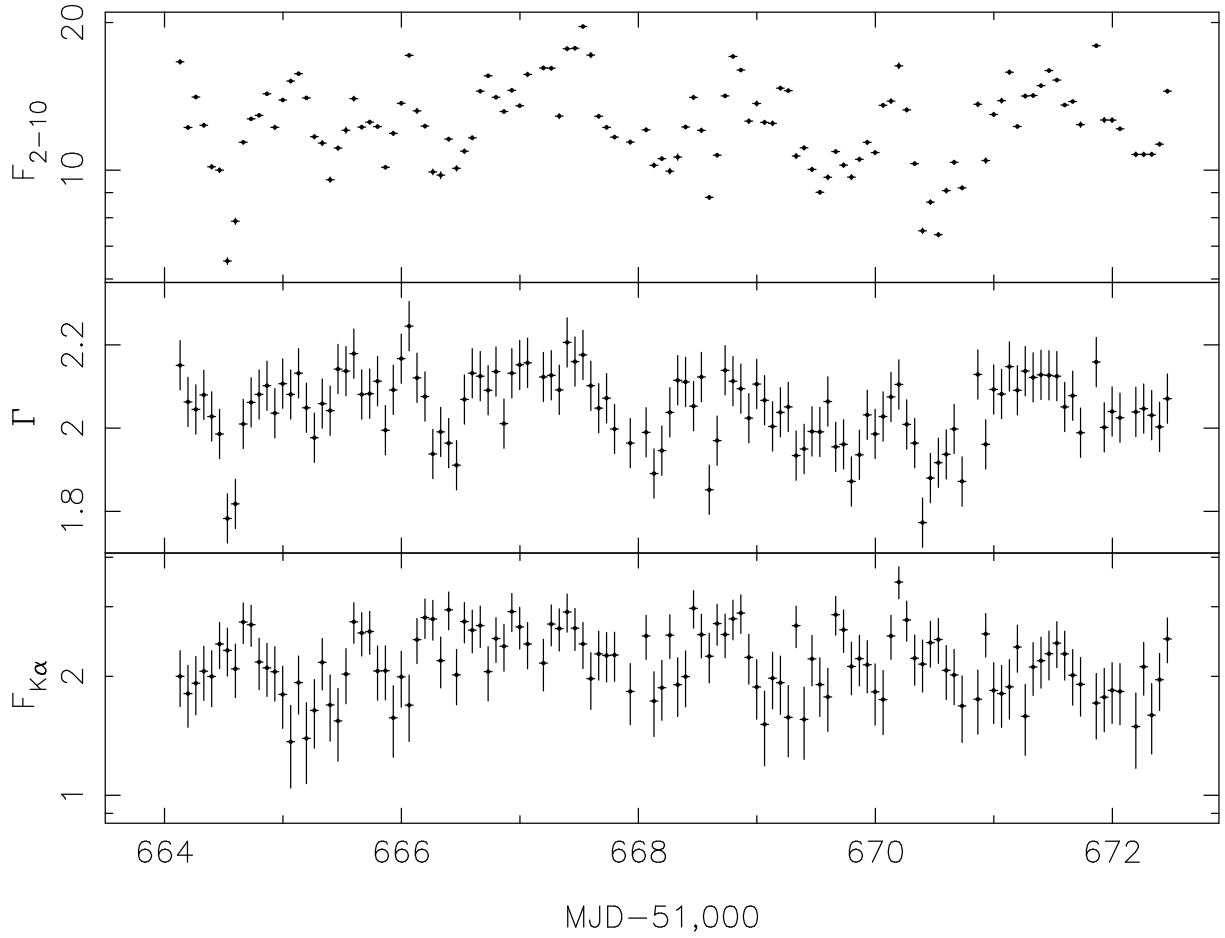

Fig. 2.— Light curves of the fit parameters derived by fitting the 120 orbital spectra with a model comprising a power-law, a Gaussian emission line and a reflection component (with fixed R). The spectral model is described in § 3.1 and the 1σ error bars are derived in § 3.3. The top panel shows the 2–10 keV light curve of MCG−6-30-15 (in ct s^{-1}) binned to match the orbit of *RXTE* (orbital period $\approx$ 96 min). The other panels show the power-law slope Γ and the iron line flux (10^{-4} photons cm^{-2} s^{-1}). Note the log scale on the y–axes.

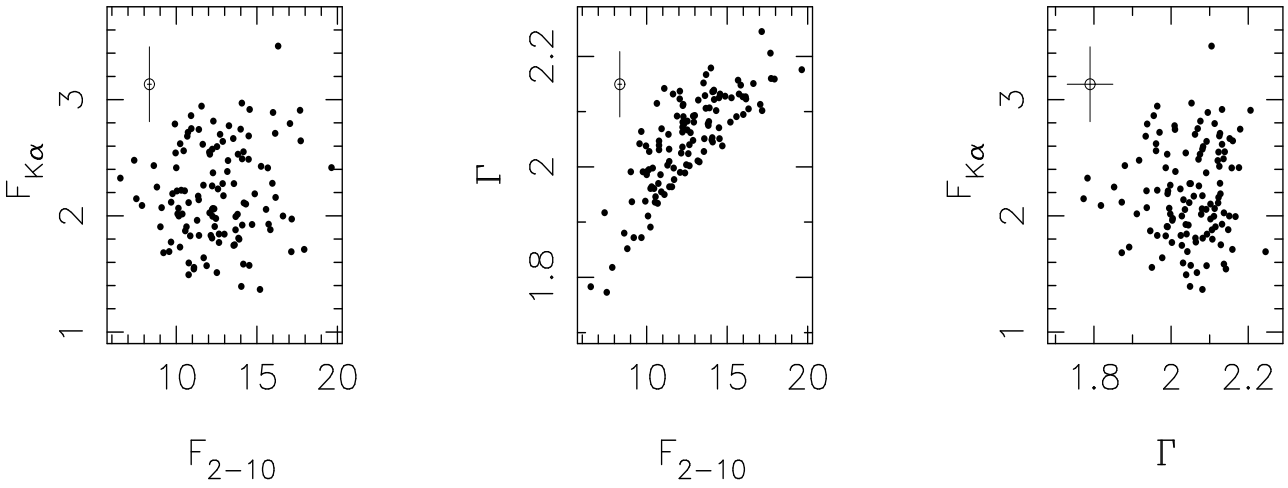

Fig. 3.— Zero-lag correlation diagrams for the data shown in figure 2. The size of the error bars, calculated in § 3.3, are indicated in the top left corner of each panel. The only strong correlation observed is between Γ and F_{2-10}.

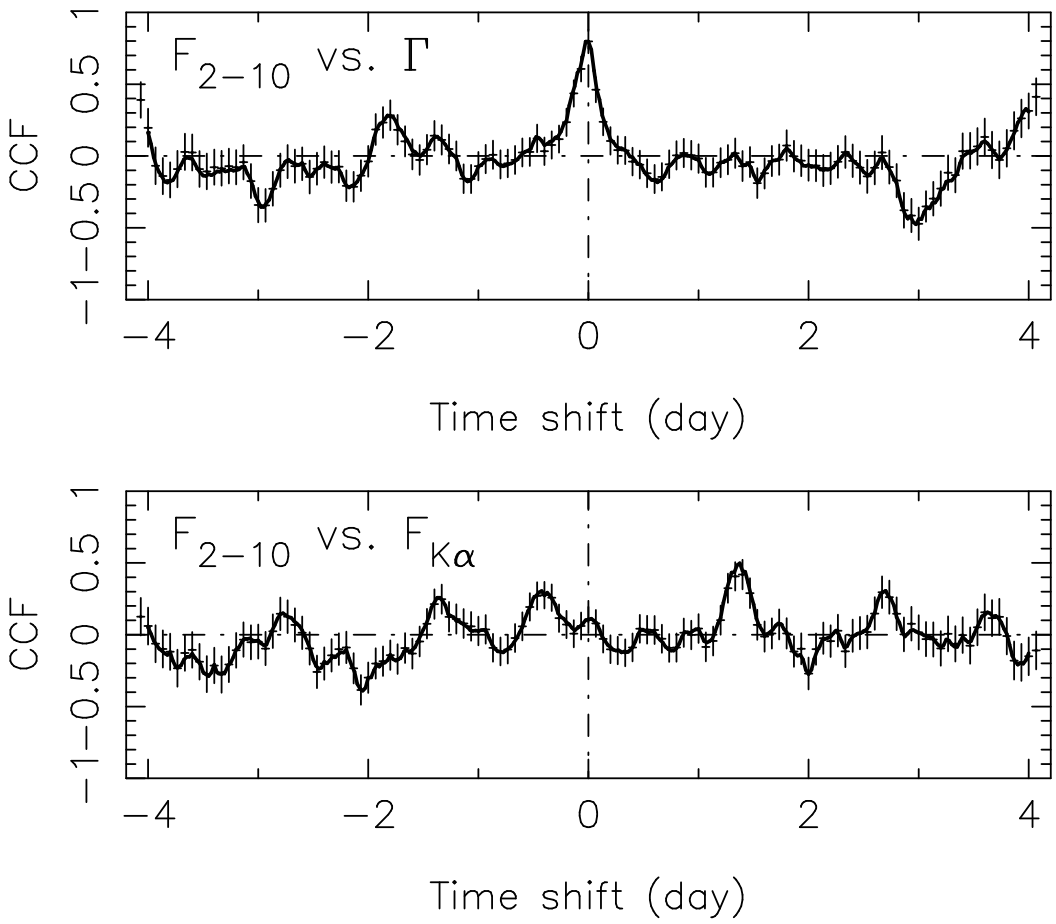

Fig. 4.— Cross-correlation functions for F_{2-10} against Γ (top panel) and against $F_{K\alpha}$ (bottom panel). The solid line refers to the interpolated correlation function while the error bars refer to the discrete correlation function. Only F_{2-10} against Γ shows a significant correlation.

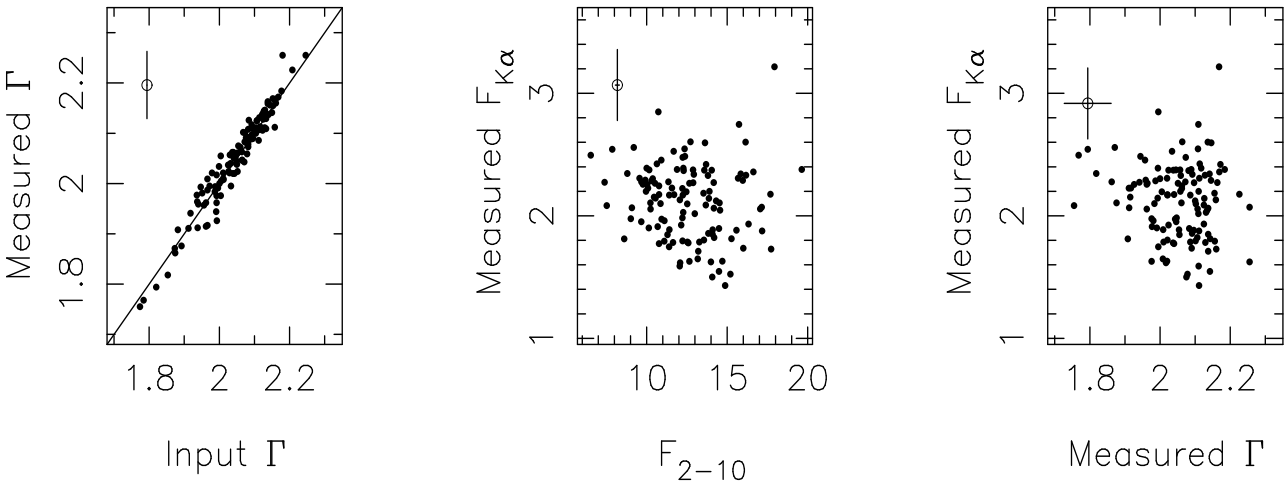

Fig. 5.— Correlation diagrams for a simulated dataset. The values of Γ and F_{2-10} were taken from the real data but $F_{K\alpha}$ was constant. Again the error bars are calculated as in § 3.3. There are no spurious correlations between the measured parameters and $F_{K\alpha}$ is consistent with constant (the scatter is much smaller than in Figure 3).

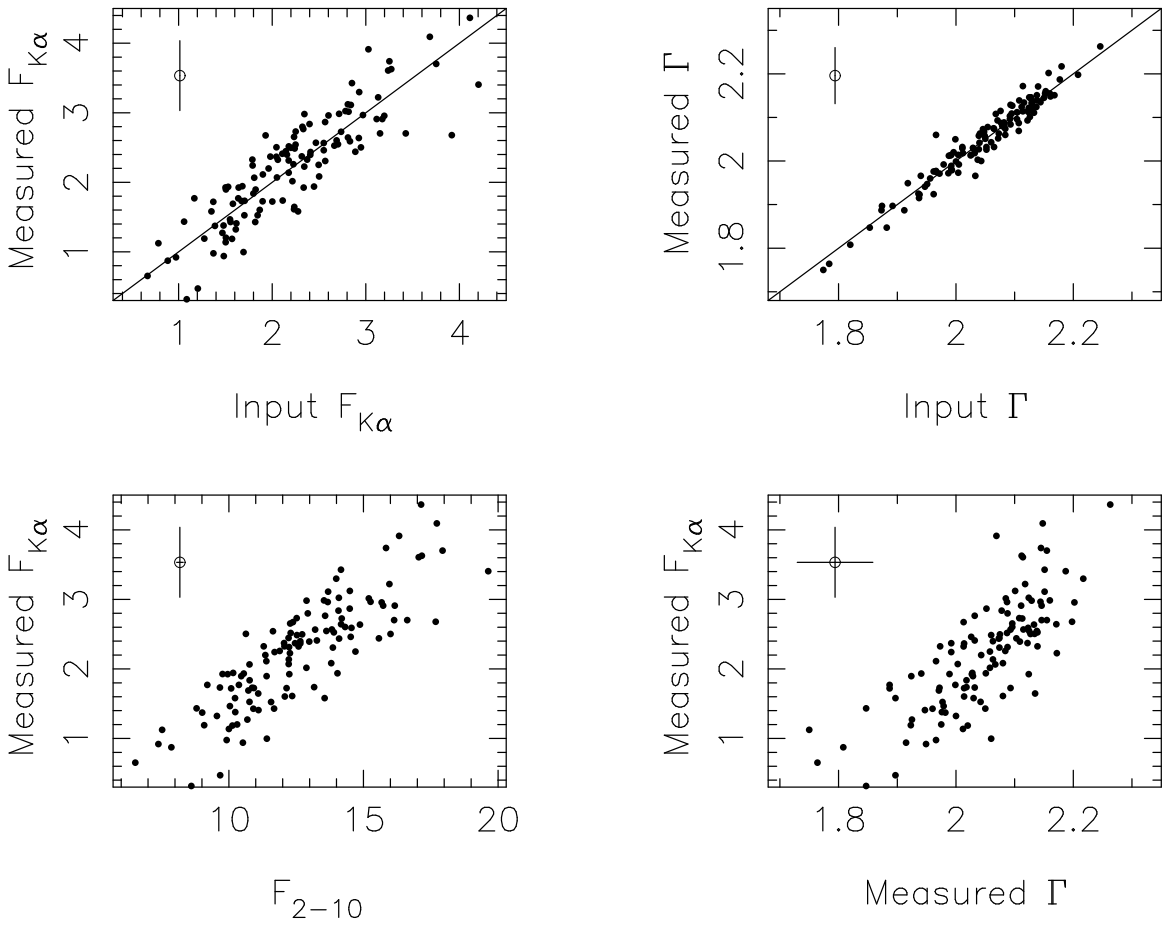

Fig. 6.— Correlation diagrams for a simulated dataset. The values of Γ and F_{2-10} were taken from the real data and $F_{K\alpha}$ is proportional to F_{2-10}. The correlation between $F_{K\alpha}$ and F_{2-10} and is clearly well recovered (and as a result, a secondary correlation between $F_{K\alpha}$ and Γ is apparent).

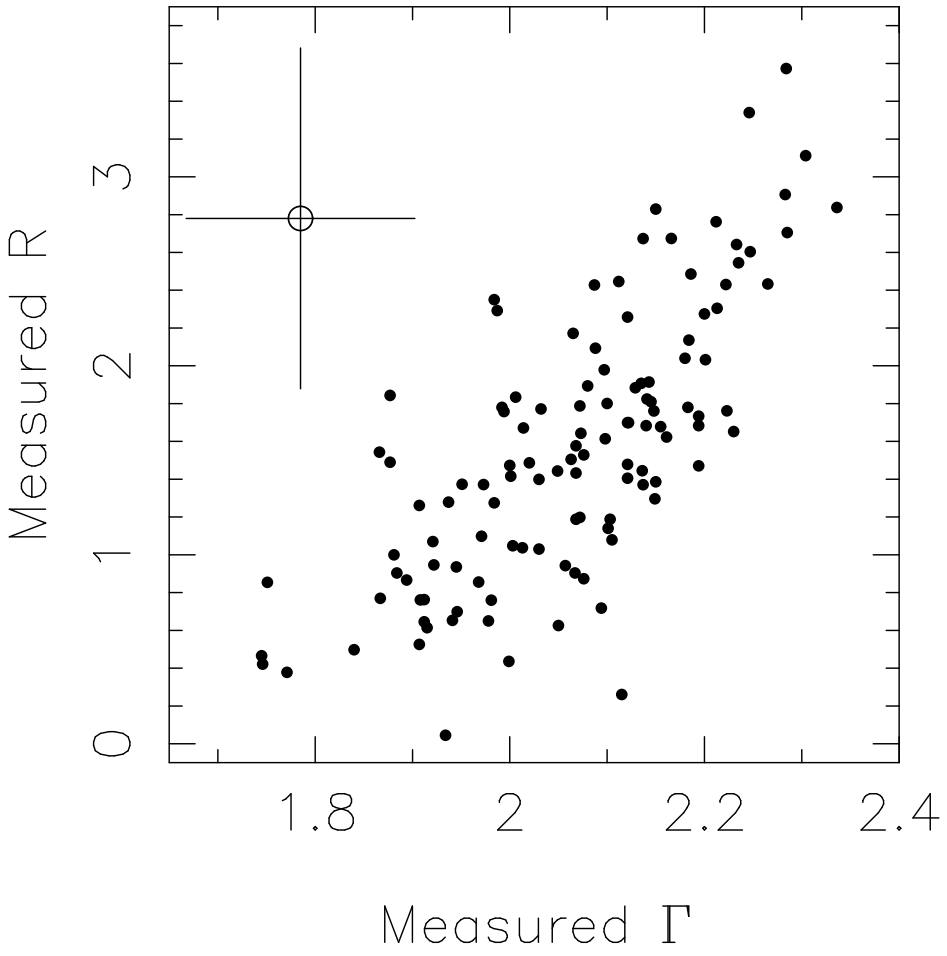

Fig. 7.— Correlation between the values of Γ and R measured from simulated data with constant $R = 1.42$. As R is fixed, there should be no correlation between Γ and R. The errors have been determined using the conservative approach outlined in § 3.3. The fact that there is a clear correlation indicates a bias in the simultaneous determination of R and Γ, and thus any observed correlation between Γ and R must be considered with caution.